# *A Theoretical Analysis of Thixotropic Parameter's Influence on Blood Flow Through Constriction*

**Nazish Shahid**

**Arabian Journal for Science and Engineering**

ISSN 2193-567X

Arab J Sci Eng
DOI 10.1007/s13369-018-3603-6

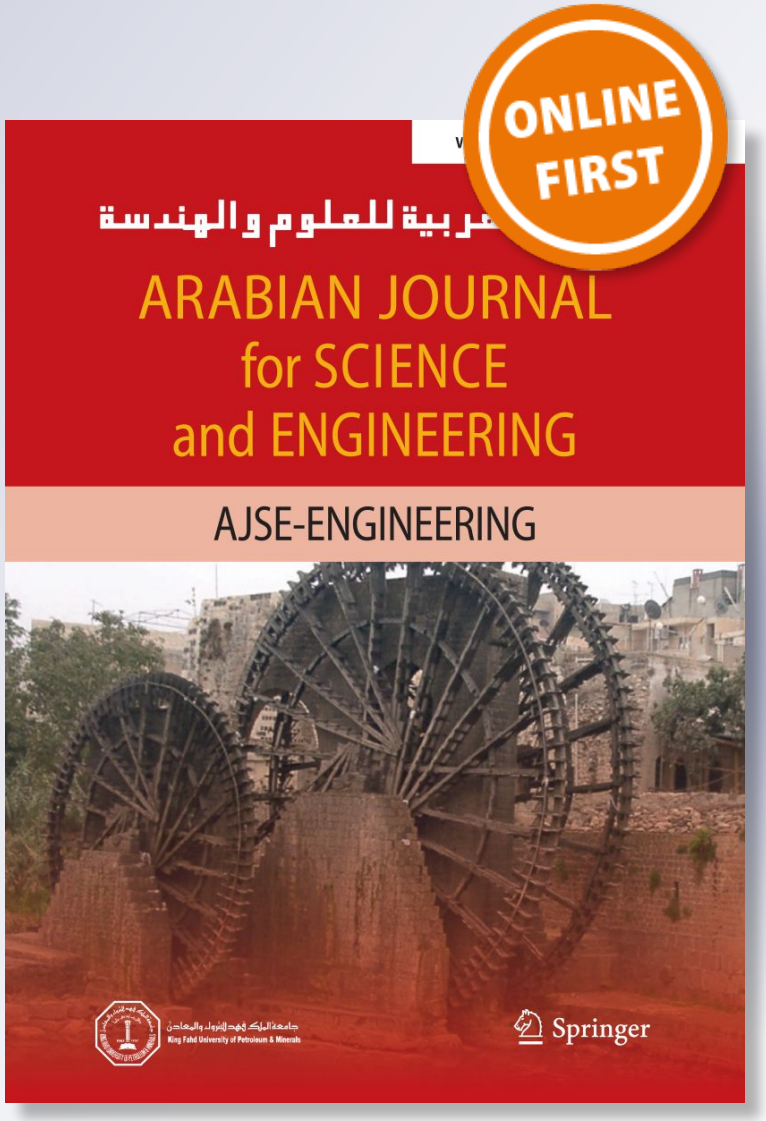


Springer

Arabian Journal for Science and Engineering
https://doi.org/10.1007/s13369-018-3603-6

RESEARCH ARTICLE - MECHANICAL ENGINEERING

# A Theoretical Analysis of Thixotropic Parameter's Influence on Blood Flow Through Constriction

Nazish Shahid[1,2]

Received: 29 November 2017 / Accepted: 9 October 2018


**Abstract**
This study has been prepared to investigate the changes in the dynamics of blood flow through a stenosed tapered artery owing to a change in structural parameter λ of thixotropic model. Following the time evolution range of this parameter as [0,1] for transient shear flows, the effects of λ on axial velocity, shear stress, flow rate and resistance to flow have been probed. Analytical expressions of axial velocity and shear stress have been obtained along with numerical computation of pressure gradient by means of continuity equation. The evolution of system with respect to time, $t$ has been investigated in order to study the changes in dynamics of flow at certain times. A comparison of axial velocity profiles for some values of λ has been made to obtain profiles for Power law fluid and Newtonian fluid model. The inclination of velocity profiles for $0.5 \leq \lambda \leq 1$ towards experimental velocity profiles has been suggested by means of comparison with available results in history. This analysis has also been prepared as a foundational step of construction of an artificial channel with constriction and of adaptation of most suitable modelling of blood flow such that the findings of the parameter λ and its influence on flow can be incorporated experimentally for induction of decreased wall stress.

**Keywords** Thixotropy · Blood flow · Time dependence · Constricted channel · Axial velocity · Yield stress

## 1 Introduction

It has been established that one of the numerous causes to alter and influence the arterial blood rheology is development of stenosis. The progression of stenosis not only advances the vascular malfunction but it also adds to the additional complexity while diseased blood through this vessel is considered. A good number of experimental, theoretical and computational investigations of flow modelling through stenosed arteries have profoundly strengthened the understanding of various models' parameters and conditions affecting flow in substantial ways. Young [1,2] and Young and Tsai [3] investigated the effects of time-dependent stenosis on flow through a tube and steady blood flow characteristics through stenosed arteries. Pulsatile flow of blood through various stenosed mediums taking into account body acceleration and magnetic field effects using Newtonian modelling has been probed by [4–13]. An analytical demonstration of flow pattern dependence on geometry of stenosed channel and Reynolds number was made by Smith [14]. A computational scheme was introduced by Deshpande et al. [15] to study steady Newtonian flow through an axisymmetric vascular stenosis.

Due to structural limitation exhibited by stenosis and low shear-rate blood flow in critical region, an analysis of non-Newtonian blood flow modelling was imperative. Many aspects of non-Newtonian behaviour along with various geometrical description of stenosis have been discussed in detail by considering blood as Casson fluid, Power law fluid and Herschel–Bulkley fluid [16–28]. In addition to being non-Newtonian, blood is also characterised by viscoplasticity and thixotropy. These characteristics have been manifested in dense suspension of red blood cells, plasma, leucocytes and platelets, etc. The properties of aggregation of red blood cells at low shear rates and their disintegration during flow refers to shear-thinning characteristics of blood and yield stress. Aggregation of red blood cells in rouleaux structure at low shear rate and then breakdown of this state during

✉ Nazish Shahid
nash_shhd@hotmail.com; nshahid@princeton.edu; nazishshahid@fccollege.edu.pk

[1] Department of Mathematics, Forman Christian College, A Chartered University, Lahore 54600, Pakistan

[2] Department of Mechanical and Aerospace Engineering, Princeton University, Princeton, NJ 08540, USA

Published online: 22 October 2018

flow or at high shear rates explains the dependence of flow on varying time scales, thus referring to time-dependent viscosity (thixotropy) of blood. To include the characteristics of thixotropy in blood flow rheology, some experimental investigations were carried out by Bureau [29,30], Dintenfass [31], Cokelet et al. [32], Chien et al. [33], Merril and Pelletier [34–36], Thurston [37,38]. These were mostly focused on simple shear steady-state flow, demonstrating the existence of blood yield stress and transition of non-Newtonian flow into Newtonian flow at higher shear rates. Though steady-state low shear rate study gave good insight into non-Newtonian, viscoplastic thixotropic characteristics of blood but its limitation to describe complex thixotropic and viscoelastic properties was a major drawback.

Development of some non-Newtonian models such as Casson and Herschel–Bulkley models were preferred to Power law fluid model (without yield stress) to incorporate the characteristics of viscoelasticity and viscoplasticity of blood along with thixotropy [39–41]. But due to viscoelastic origin of exact equations, they were not able to interpret the characteristics of blood such as yield stress. Some significant results regarding the demonstration of all above properties of blood were presented by Anand and Rajagopal [42] and Ananad et al. [43] using Oldroyd-B model accounting for only zero shear-rate viscosity or smooth transitions of viscosity at low shear rates. Regarding the study of blood flow through stenosed arteries, some profound results were obtained. A multiple-stenosis study presenting one-dimensional analysis of non-Newtonian blood flow using Casson model was developed by Pincombe et al. [44]. Similarity of Herschel–Bulkley and Casson modelling of non-Newtonian blood flow over the validity range of Casson model was discussed by Blair and Spanner [45]. Priyadharshini and Ponalagusamy [46] investigated many physiological properties of blood flow through stenosed and dilated arteries using Herschel–Bulkley model. Considering the bifurcating nature of blood vessels at frequent intervals and varying diameters of channel, Whitemore [47], Manton [48] and Mandal [49] have presented analysis of tapering effects on flow and structural time dependence of stenosis.

To explicitly account for the characteristics of yield stress in a viscoplastic system, some thixotropic models were generated. Mujumdar et al. [50] and Dullaert [51] have expressed characteristics of thixotropy using some structural models at phenomenological level. But Mewis and Wagner [52] have explicitly described a thixotropic model linking a structural parameter to yield stress and time-dependent viscosity. In this description of model, thixotropy is accounted for by time evolution of the structural parameter that further satisfied the relaxation equation. This relaxation equation is composed of structure recovery part (yield stress) and shear-induced structure part referring to thixotropy. An experimental insight regarding blood rheology by Apostolidis and Beris [53] validated that Casson viscoplastic model was the most suitable one for steady-state shear flow, but its limitation was already acknowledged in terms of missing out on transient and time-dependent nature of colloidal blood suspension by Mewis [54]. Also due to the limitation of Herschel–Bulkley and Bingham models [55] to fully capitalise on elasticity, they were not considered among the most suitable for blood flow description.

Most recently, considering the lack of attempts to describe the transient blood rheology and systematically approach the concept of higher shear-rate flow, Apostolidis et al. [56] have modified the Delaware model, developed by Mujumdar el al. [50] for a thixotropic concentrated ceramic suspension. In this model, a single structural parameter $\lambda$ in constitutive equation is considered to be linking yield stress and thixotropy. In a subsequent development of thixotropic model, the elastic contribution to shear stress was substituted by a moduls function of this parameter times an elastic strain, where the evolution of elastic strain was described in terms of imposed shear rate. Apostolidis and Anthony [53] further modified this thixotropic model by employing a relation between $\lambda$ and zero shear-rate and infinite shear-rate limiting value for maximum elastic strain supported within the material. This proposed relation led to a remarkable result relating the factors of plastic strain and shear rate. The validation of this model was reached by reducing this models' results to Casson fluid steady-state results for low shear rates. It was also observed that in the limit of higher shear rates, thixotropic model was reduced to Newtonian fluid. Thus, an approach of linking a parameter ($\lambda$), characterising the material, with yield stress and thixotropy, such that evolution of this parameter is decomposed into recovery and structure breakdown parts, reflecting on transient flow properties of blood at both higher and lower shear rates. Modification of thixotropic model done by Apostolidis et al. [56] employing structural parameter $\lambda$ signalled to obtain transient shear flow mechanism and deduction of steady-state shear flow results for limiting values of $\lambda$. However, validation of this approach using phenomenological equations by obtaining exact results matching the experimental data was yet to be done. To the best of our knowledge, investigation of transient blood flow dynamics using thixotropic model has not been carried out before.

In the present article, the dynamics of non-Newtonian blood flow through stenosed artery have been discussed in conjunction with single structural parameter '$\lambda$' of thixotropic model. To what extent, flow properties are influenced by this parameter has been thoroughly investigated. Following [56], this parameter's range as it evolves in time has been chosen as [0, 1] for which limiting cases have been derived on both ends. An analytical expression of axial velocity has been obtained. However, pressure gradient has been obtained numerically using MATLAB. The unsteady nature

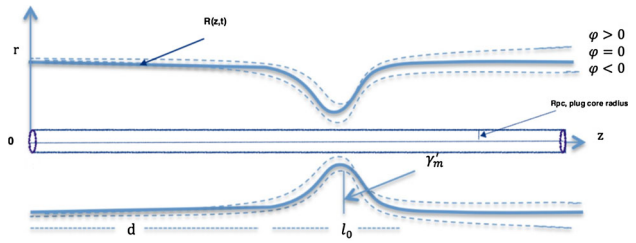


**Fig. 1** A 2-dimensional stenosed, tapered channel

of blood flow has been probed and discussed by means of analytical expressions as well as by using numerical data. This analysis has also been motivated to observe dynamical differences caused by the parameter λ here as compared to the Herschel–Bulkley fluid modelling [46]. Physical characteristics of blood flow in conjunction with the effects of λ on them have been discussed through graphical illustration.

## 2 Geometry of Flow

We consider a cylindrical coordinate system $(r, \theta, z)$ to depict blood flow through an elastic tapered vessel with mild stenosis such that $r$ is taken along the radial direction of the vessel, $\theta$ to be the circumferential direction and $z$-axis is considered to be along the axis of channel, perpendicular to the radial axis. The unsteady, incompressible and non-Newtonian blood through this tapered vessel (Fig. 1) is characterised by Thixotropic modelling . A 2D geometric depiction of elastic arterial segment has been included where tapering of vessel is denoted by an angle, different from circumferential direction. The geometry of stenosed artery is described as [49]

$$\bar{R}(z,t) = \begin{cases} \left((m' z + R_0) - \frac{\gamma_{m'} \sec\phi (z-d)}{\frac{l_0^2}{4} - \gamma_{m'}^2 \sin^2\phi}(l_0 - (z-d))\right)\bar{\eta}(t), \\ \quad \text{for} \quad d \le z \le d + l_0 \\ (m' z + R_0)\bar{\eta}(t), \quad \text{Otherwise} \end{cases} \tag{1}$$

where $\bar{R}(z,t)$ represents the radius of tapered artery in the stenotic region, $l_0$ length of stenosis, $d$ position of stenosis, $R_0$ constant radius of non-tapered artery in non-stenotic region, $\phi$ angle of tapering ($\phi < 0$ for converging tapering, $\phi > 0$ for diverging tapering and $\phi = 0$ for no-tapering), $\gamma_{m'}$ height of stenosis at $z = d + \frac{l_0}{2}$ (with no-tapering) and $m' = \tan\phi$ denotes the slope of tapering.

Also, $\bar{\eta}(t)$ is described as

$$\bar{\eta}(t) = 1 - g\{\cos(\omega t) - 1\}\mathrm{e}^{-g\omega t}$$

where $\omega = 2\pi f$ defines angular frequency such that $f$ represents pulse frequency and $g$ is a constant defining amplitude of small oscillations.

## 3 Mathematical Modelling

The governing equations of momentum for $r$-component and $z$-component and the continuity equation corresponding to two-dimensional, unsteady, non-Newtonian and axisymmetric flow through tapered artery with stenosis have been described as

$$\rho\left(\frac{\partial u}{\partial t} + u\frac{\partial u}{\partial r} + w\frac{\partial u}{\partial z}\right) = -\left(\frac{1}{r}\frac{\partial (r\tau_{rr})}{\partial r} + \frac{\partial (\tau_{zr})}{\partial z}\right) - \frac{\partial p}{\partial r}, \tag{2}$$

$$\rho\left(\frac{\partial w}{\partial t} + u\frac{\partial w}{\partial r} + w\frac{\partial w}{\partial z}\right) = -\left(\frac{1}{r}\frac{\partial (r\tau_{rz})}{\partial r} + \frac{\partial (\tau_{zz})}{\partial z}\right) - \frac{\partial p}{\partial z}, \tag{3}$$

$$\frac{\partial u}{\partial r} + \frac{u}{r} + \frac{\partial w}{\partial z} = 0, \tag{4}$$

where $u = u(r, z, t)$ and $w = w(r, z, t)$ are radial and axial components of velocity. And $\rho$ describes density of flow. The constitutive equations is [52,53,56]

$$\tau = \lambda\tau_y + (1-\lambda)\bar{k}(-\dot{\gamma})^n, \quad \tau > \tau_y \tag{5}$$

where $\tau = |\tau_{rz}| = -\tau_{rz}$ and $0 < \lambda < 1$. And

$$\dot{\gamma} = 0, \quad \tau \le \tau_y \tag{6}$$

Also, $\tau, \dot{\gamma}$, $\tau_y$, $\bar{k}$ and $n$ are shear stress, rate of deformation, yield stress, consistency index and flow behaviour index, respectively. The corresponding boundary conditions are

$$\begin{aligned} &w(r,z,t) = 0 \ \text{ at } \ r = \bar{R}(z,t); \\ &\tau_{rz}(r,z,t) = 0 \ \text{ at } \ r = 0 \end{aligned} \tag{7}$$

Following non-dimensional variables are considered

$$t^* = \frac{w_0 t}{l}, \quad z^* = \frac{z}{l}, \quad w^* = \frac{w}{w_0}, \quad u^* = \frac{u}{u_0}, \quad p^* = \frac{p}{p_0},$$
$$w_0 = \frac{u_0 l}{R_0}, \quad t_0 = \frac{l}{w_0}, \quad \tau_{rz}^* = \frac{R_0\tau_{rz}}{\mu w_0}, \quad \tau_{zz}^* = \frac{l\tau_{zz}}{\mu w_0},$$
$$p_0 = \frac{\mu l w_0}{R_0^2}, \quad R^* = \frac{\bar{R}}{R_0}, \quad d^* = \frac{d}{l}, \quad l_0^* = \frac{l_0}{l}, \quad \omega^* = \frac{t_0\omega}{2\pi},$$
$$\gamma_{m'}^* = \frac{\gamma_{m'}}{R_0}, \quad m = \frac{m' l}{R_0}, \quad Q^* = \frac{\bar{Q}}{w_0 R_0^2}, \quad R_e = \frac{\rho R_0 w_0}{\mu},$$

$$\tau_y^* = \frac{R_0\tau_y}{\mu w_0}, \quad K = \frac{\bar{k}}{\mu}\left(\frac{w_0}{R_0}\right)^{n-1}, \tag{8}$$

where $'l'$ is the length of artery. Using non-dimensional quantities (8), very small Reynolds number, $R_e$, and

$$R_0 \ll l,$$

we obtain (ignoring $*$)

$$-\frac{\partial p}{\partial z} = \frac{1}{r}\frac{\partial(r\tau_{rz})}{\partial r}, \tag{9}$$

$$\frac{\partial p}{\partial r} = 0, \tag{10}$$

$$\tau = \lambda\tau_y + (1-\lambda)K\left(-\frac{\partial w}{\partial r}\right)^n, \tag{11}$$

$$\frac{\partial u}{\partial r} + \frac{u}{r} + \frac{\partial w}{\partial z} = 0, \tag{12}$$

with boundary conditions

$$w(r,z,t) = 0 \ \text{ at } \ r = R(z,t); \ \ \tau_{rz}(r,z,t) = 0 \ \text{ at } \ r = 0. \tag{13}$$

Also, the wall geometry is

$$R(z,t) = \left\{(mz+1) - \frac{4\gamma_m \sec\phi(z-d)(l_0-(z-d))}{l_0^2}\right\}\eta(t), \tag{14}$$

for $d \le z \le d + l_0$, where

$$\eta(t) = 1 - g\{\cos(2\pi\omega t) - 1\}\mathrm{e}^{-2\pi g\omega t}. \tag{15}$$

## 4 Analytical Expressions of Velocity and Wall Shear Stress

Integrating Eq. (12) with respect to $r$ from $r = 0$ to $r = R(z,t)$, we obtain

$$R(z,t)\frac{\partial R(z,t)}{\partial t} + \frac{\partial}{\partial z}\int_0^R r w(r,z,t)\mathrm{d}r = 0. \tag{16}$$

We make a coordinate transformation [49] using $\frac{r}{R(z,t)} = x$ and obtain from Eqs. (9), (10), (11) and (16) the following

$$-\frac{\partial p}{\partial z} = \frac{1}{xR(z,t)}\frac{\partial(x\tau_{xz})}{\partial x}, \tag{17}$$

$$\frac{\partial p}{\partial x} = 0, \tag{18}$$

$$\tau = \lambda\tau_y + \frac{(1-\lambda)K}{R^n(z,t)}\left(-\frac{\partial w}{\partial x}\right)^n \tag{19}$$

$$R(z,t)\frac{\partial R(z,t)}{\partial t} + \frac{\partial}{\partial z}\left(R^2(z,t)\int_0^1 x w(x,z,t)\mathrm{d}x\right) = 0 \tag{20}$$

with boundary conditions

$$w(x,z,t) = 0 \ \text{ at } \ x = 1; \ \ \tau_{xz}(x,z,t) = 0 \ \text{ at } \ x = 0. \tag{21}$$

Also, we have

$$\frac{\partial w}{\partial x} = 0, \quad 0 \le x \le R_{\mathrm{pc}} \tag{22}$$

$R_{\mathrm{pc}}$, being the radius of plug-core region.

Solving Eq. (17) with $(21)_2$, we obtain an expression of shear stress

$$\tau_{xz} = \frac{xR(z,t)}{2}\left(-\frac{\partial p}{\partial z}\right) \tag{23}$$

And the expression for wall shear stress ($x = 1$) is

$$\tau_{ws} = \frac{R(z,t)}{2}\left(-\frac{\partial p}{\partial z}\right) \tag{24}$$

Solving Eq. (19) with $(21)_1$ and (23), we get an expression for axial velocity

$$w(x,z,t) = \frac{nR(z,t)}{(n+1)(M+2\lambda\tau_y)(2K(1-\lambda))^{\frac{1}{n}})} \times\left\{M^{\frac{n+1}{n}} - \left(Mx + 2\lambda\tau_y(x-1)\right)^{\frac{n+1}{n}}\right\} \tag{25}$$

where $M = R(z,t)(-\frac{\partial p}{\partial z}) - 2\lambda\tau_y$ and $R_{\mathrm{pc}} \le x \le R(z,t)$. And the velocity in plug-core region is

$$w_{\mathrm{pc}}(x,z,t) = \frac{nR(z,t)}{(n+1)(M+2\lambda\tau_y)(2K(1-\lambda))^{\frac{1}{n}}} \left\{M^{\frac{n+1}{n}}\right\} \tag{26}$$

for $0 < x \le R_{\mathrm{pc}}$ and $R_{\mathrm{pc}} = \frac{2\lambda\tau_y}{R(z,t)\frac{-\partial p}{\partial z}}$.

These expressions of axial velocity have been written in the form to obtain approximations for pressure gradient easily. We write Eq. (20) in the form

$$\frac{1}{2}\frac{\partial A(z,t)}{\partial t} + \frac{\partial}{\partial z}\left(A(z,t)\int_0^1 x w(x,z,t)\mathrm{d}x\right) = 0 \tag{27}$$

where $A(z,t) = R^2(z,t)$.

Volume flow rate is defined as

$$\bar{Q} = 2\pi\int_{r=0}^{r=\bar{R}(z,t)} r w(r,z,t)\mathrm{d}r \tag{28}$$

which in non-dimensional form (ignoring $*$) can be written as

$$Q(z,t) = 2\pi \int_{r=0}^{r=R(z,t)} r w(r,z,t) \mathrm{d}r \tag{29}$$

Equation (29) in terms of $x$ coordinate is

$$Q(z,t) = 2\pi\ A(z,t) \int_0^1 x w(x,z,t) \mathrm{d}x \tag{30}$$

## 5 Numerical Analysis of Pressure Gradient

We use Eq. (27) to obtain an equation of pressure gradient. Integrating Eq. (27) with respect to $z$, we get

$$Q(z,t) = -\pi \int \frac{\partial A(z,t)}{\partial t} \mathrm{d}z + C(t) \tag{31}$$

To get an expression of $C(t)$, the starting pressure gradient at $z = 0$ has been set to '1'. This pressure gradient at the start of channel is set randomly, but it is also very well in consistency with required pressure gradient for flow propagation in the artery. Using initial pressure gradient and Eqs. (30) and (31), we obtain

$$\begin{aligned} C(t) = & \frac{2\pi n}{2(n+1)(2n+1)(3n+1)(2K(1-\lambda))^{\frac{1}{n}}} \\ & \times \Big\{ 2n^2 (T(t) - 2\lambda\tau_y)^{\frac{3n+1}{n}} \\ & - 2n(3n+1)T(t)(T(t) - 2\lambda\tau_y)^{\frac{2n+1}{n}} \\ & + (2n+1)(3n+1)T^2(t)(T(t) - 2\lambda\tau_y)^{\frac{n+1}{n}} \Big\} \end{aligned} \tag{32}$$

where

$$\begin{aligned} T(t) &= R(z,t)|_{z=0} \\ &= \left\{ 1 + \frac{4\gamma_m \sec\phi (d)(l_0 + d)}{l_0^2} \right\} \eta(t), \end{aligned} \tag{33}$$

for $d \le z \le d + l_0$ and $\eta(t)$ is given by Eq. (15). Simplifying Eq. (31) with Eqs. (14), (30), (32) and (33), we obtain an expression

$$\begin{aligned} & (n+1)(2n+1)M^{\frac{3n+1}{n}} + 4\lambda\tau_y (n+1)(3n+1)M^{\frac{2n+1}{n}} \\ & + 4\lambda^2\tau_y^2 (2n+1)(3n+1)M^{\frac{n+1}{n}} = \frac{\zeta(n,\lambda,K)(M + 2\lambda\tau_y)^3}{2\pi R^3(z)} \\ & \times \Big\{ C(t) - \frac{2\pi}{l_0^4} \left( \frac{a^2 z^5}{5} + \frac{2abz^4}{4} + \frac{(2ac + b^2)z^3}{3} + bcz^2 + c^2 z \right) \\ & \times \times \eta(t)\dot{\eta}(t) \Big\} \end{aligned} \tag{34}$$

where

$$\begin{aligned} \zeta(n,\lambda,K) &= \frac{2(n+1)(2n+1)(3n+1)(2K(1-\lambda))^{\frac{1}{n}}}{n}, \\ M &= R(z,t)(-\frac{\partial p}{\partial z}) - 2\lambda\tau_y, \\ a &= 4\gamma_m \sec\phi, \\ b &= ml_0^2 - 4\gamma_m \sec\phi (l_0 + 2d), \\ c &= 4\gamma_m \sec\phi (l_0 d + d^2) + l_0^2 \end{aligned}$$

Equation (34) is numerically solved using MATLAB for values of $-\frac{\partial p}{\partial z}$ with the help of Eq. (32). We have used Matlab solver 'fzero' to calculate nonzero root $M$ of nonlinear Eq. (34) using given values of time, position, characteristic parameter, yield stress, consistency index, flow behaviour index, amplitude of small oscillation, oscillating frequency, tapering angle and length of stenosis. Determination of $M$ leads to numerical computation of pressure gradient, imposed at the given position of stenosis. Numerical values of $M$ can also be obtained through individual computation of indexing parametric function $\zeta(n, \lambda, K)$ and time-induced arterial variations $(a, b, c)$. The structure of our solutions for pressure gradient was defined within the region bounded by $R_{\mathrm{pc}}$ (plug-core region radius) and $R(z,t)$. For better projection of solutions in graphs, we made use of MATLAB optimest (optimplotx, optimplotfval). To track the response and progress of varying physical quantities through graphs, we have also used optimisation MATLAB solver (fminsearch). Finally, numerically computed values of pressure gradient were incorporated in Eqs. (23–26, 30, 35) to obtain shear stress, axial velocity, flow rate, and flow resistance.

Resistance to flow can be obtained using

$$\mho = \int_0^z \frac{\left( -\frac{\partial p}{\partial z} \right)}{Q} \mathrm{d}z \tag{35}$$

with the help of Eqs. (30) and (34).

Table 1 is constructed to display the effects of varying yield stress on pressure gradient at a given time and position of stenosis for the case of converging tapering. In general, pressure gradient is decreasing with increase in yield stress. However, it is observed that pressure gradient decreases for smaller $\lambda$ values in the range $0 \le \lambda \le 1$. Thus, larger values of $\lambda$ in Thixotropic modelling tend to play a role in increasing the velocity of fluid through constriction. Though compatibility of this pressure gradient data corresponding to changing yield stress with experimental data has yet to be studied but continuous decline in pressure gradient with increasing yield stress is consistent with the fact that the stronger yielding factors hinder the course of flow.

**Table 1** Values of pressure gradient $-\frac{\partial p}{\partial z}$ for varying yield stress $\tau_y$, time $t = 0.45$, position $z = 28$ and characteristic parameter $\lambda$

| $\tau_y$ | $\lambda = 0.1$ $-\frac{\partial p}{\partial z}$ | $\lambda = 0.5$ $-\frac{\partial p}{\partial z}$ | $\lambda = 0.7$ $-\frac{\partial p}{\partial z}$ |
|---|---|---|---|
| 0.05 | 2.3210 | 3.9613 | 4.4618 |
| 0.1 | 2.3072 | 3.9110 | 4.3962 |
| 0.4 | 2.2239 | 3.6068 | 4.0016 |
| 0.8 | 2.1109 | 3.1955 | 3.4737 |
| 1.2 | 1.2602 | 2.7756 | 2.9437 |
| 1.6 | 1.8769 | 2.3437 | 2.4104 |
| 2.0 | 1.7552 | 1.8935 | 1.8704 |
| 2.4 | 1.6297 | 1.4111 | 1.3124 |

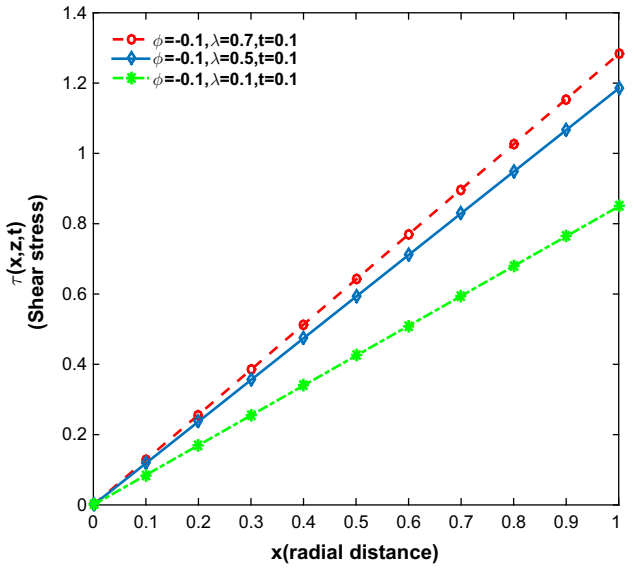


**Fig. 2** Shear stress versus radial distances for $\phi = -0.1$ at $z = 28$, $\tau_y = 1.2$, $t = 0.1$, $K = 1.2$, $\lambda = 0.7, 0.5, 0.1$

## 6 Discussion

The following numerical values of constants have been considered for graphical analysis

$$l = 50,\ \ l_0 = 16,\ \ d = 20,\ \ \gamma_m = 0.32,\ \ \omega = 6,\ \ g = 0.1,$$
$$R_0 = 0.8,\ \ n = 0.639$$

Also, some of the above numerical values have been chosen [49] in order to verify the results for Power law model through our model's approximation.

Shear stress has been profiled against radial distances in Figs. 2, 3, 4, 5, 6 and 7 for varying $\lambda$ at a position of stenosis, $z = 28$. These graphs have been obtained for converging tapering and varying time. It is observed that shear

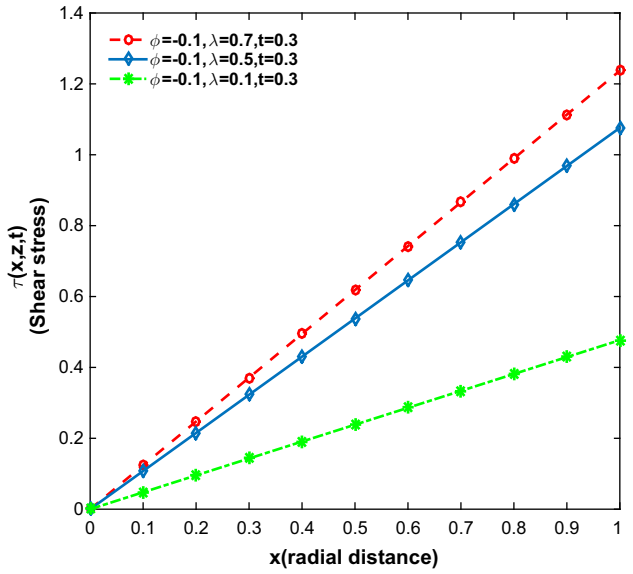


**Fig. 3** Shear stress versus radial distances for $\phi = -0.1$ at $z = 28$, $\tau_y = 1.2$, $t = 0.3$, $K = 1.2$, $\lambda = 0.7, 0.5, 0.1$

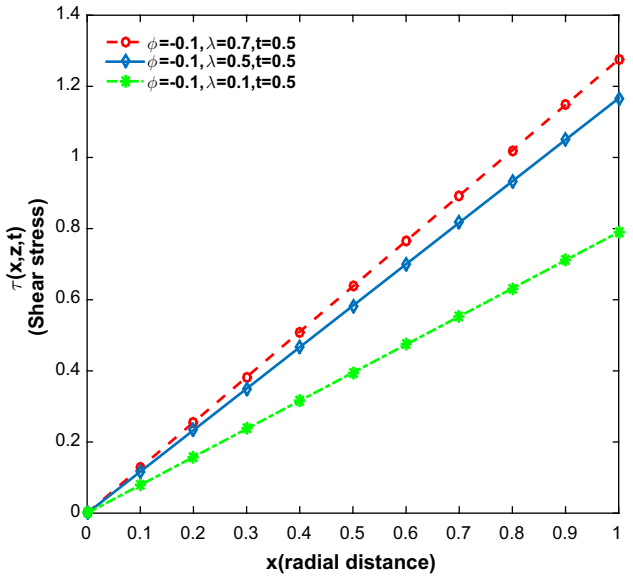


**Fig. 4** Shear stress versus radial distances for $\phi = -0.1$ at $z = 28$, $\tau_y = 1.2$, $t = 0.5$, $K = 1.2$, $\lambda = 0.7, 0.5, 0.1$

stress increases steadily corresponding to increase in radial distances, reaching to its maximum value near the boundary wall of stenosed artery. However, a keen observation of these graphs shows that the shear stress in the beginning decreases with increasing time and then it starts increasing, thus generating an oscillating pattern with respect to time. The phenomenon of decrease and increase in stress in time owes to the variation of pressure gradient accordingly. The gradual rise in pressure gradient after some time is required by fluid to flow in constricting part of the channel. Along with

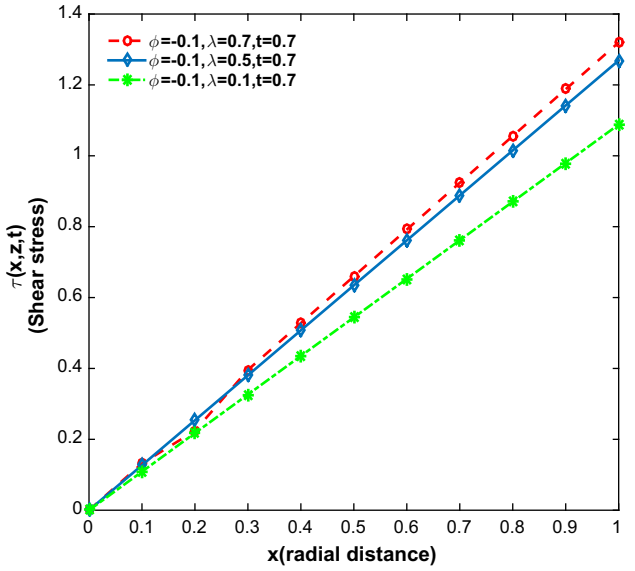


**Fig. 5** Shear stress versus radial distances for $\phi = -0.1$ at $z = 28$, $\tau_y = 1.2$, $t = 0.7$, $K = 1.2$, $\lambda = 0.7, 0.5, 0.1$

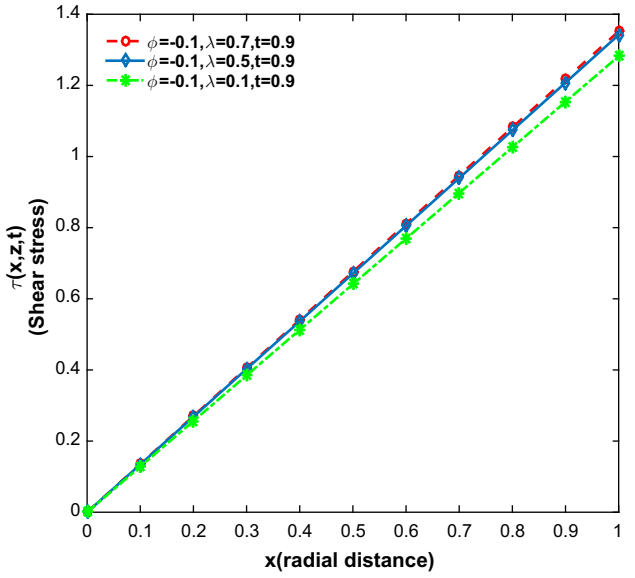


**Fig. 6** Shear stress versus radial distances for $\phi = -0.1$ at $z = 28$, $\tau_y = 1.2$, $t = 0.9$, $K = 1.2$, $\lambda = 0.7, 0.5, 0.1$

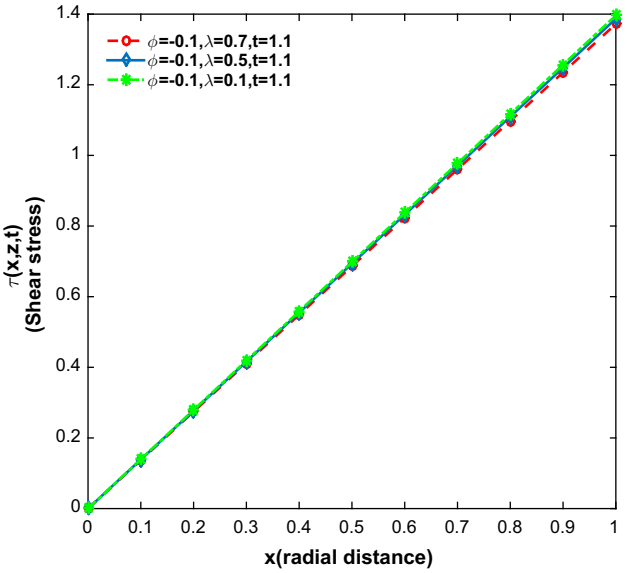


**Fig. 7** Shear stress versus radial distances for $\phi = -0.1$ at $z = 28$, $\tau_y = 1.2$, $t = 1$, $K = 1.2$, $\lambda = 0.7, 0.5, 0.1$

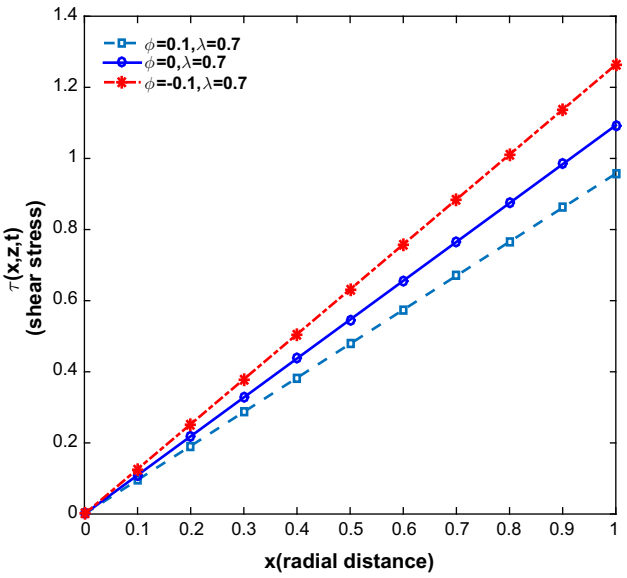


**Fig. 8** Wall shear stress versus radial distances for $\phi = 0.1, 0, -0.1$ at $z = 28$, $\tau_y = 1.2$, $t = 0.45$, $K = 1.2$, $\lambda = 0.7$

change in time, λ-values have also been observed to cause a phenomenal change in shear stress. For increasing values of λ, the shear stress increases and vice versa. Interestingly, it can be observed in these graphs that with increasing time, the difference in magnitude of shear stress for different values of λ begin to reduce causing the curves to coincide for all values of λ (Fig. 7).

Figures 8, 9 and 10 describe the variation of magnitude of shear stress at a given time and position of stenosis for converging, diverging and no-tapering of channel. It has been noted that shear stress for converging tapering exceeds the shear stress for diverging and no-tapering. The fact that higher pressure gradient is required for fluid to pass through constricting part of the channel contributes to higher stress imposed on boundary wall. A direct relation of shear stress and the parameter λ has also been displayed in these images.

Figures 11, 12, and 13 express how axial velocity is varying with change in radial distance at a stenosis position $z = 28$ and a given time. The change in velocity of fluid

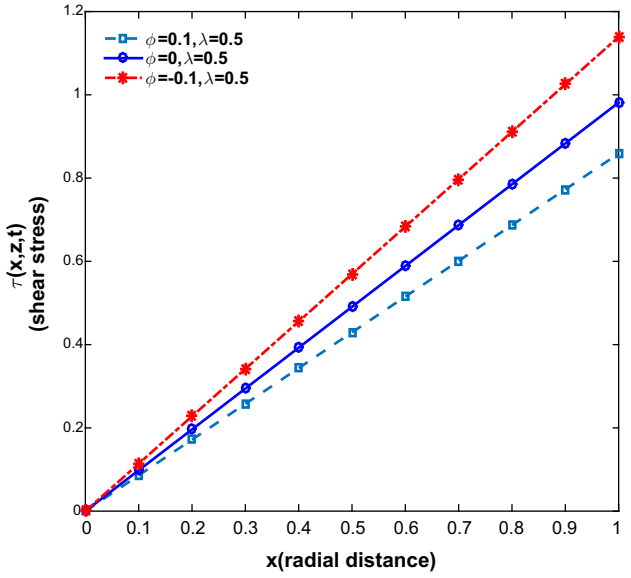


**Fig. 9** Wall shear stress versus radial distances for $\phi = 0.1, 0, -0.1$ at $z = 28$, $\tau_y = 1.2$, $t = 0.45$, $K = 1.2$, $\lambda = 0.5$

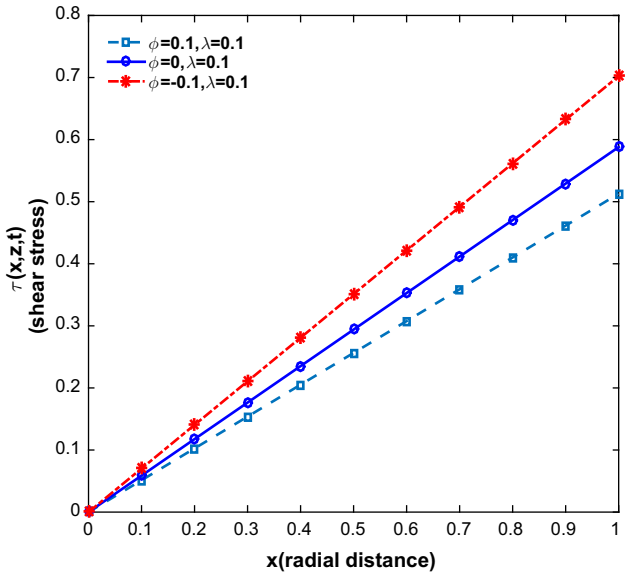


**Fig. 10** Wall shear stress versus radial distances for $\phi = 0.1, 0, -0.1$ at $z = 28$, $\tau_y = 1.2$, $t = 0.45$, $K = 1.2$, $\lambda = 0.1$

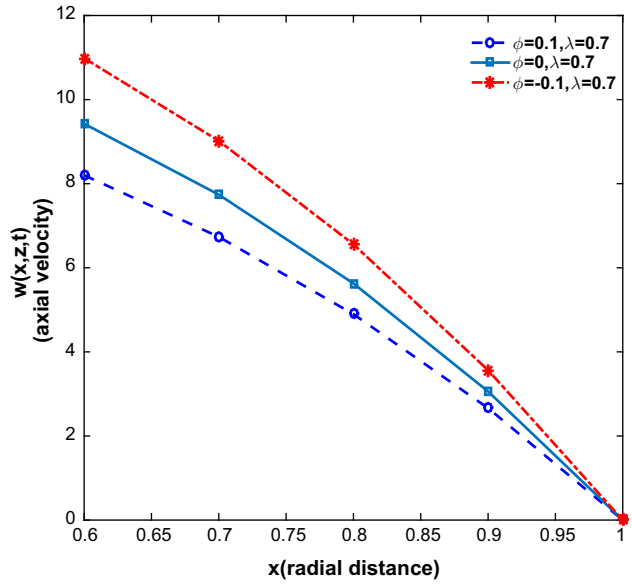


**Fig. 11** Axial velocity versus radial distances for $\phi = 0.1, 0, -0.1$ at $z = 28$, $\tau_y = 1.2$, $t = 0.45$, $K = 1.2$, $\lambda = 0.7$

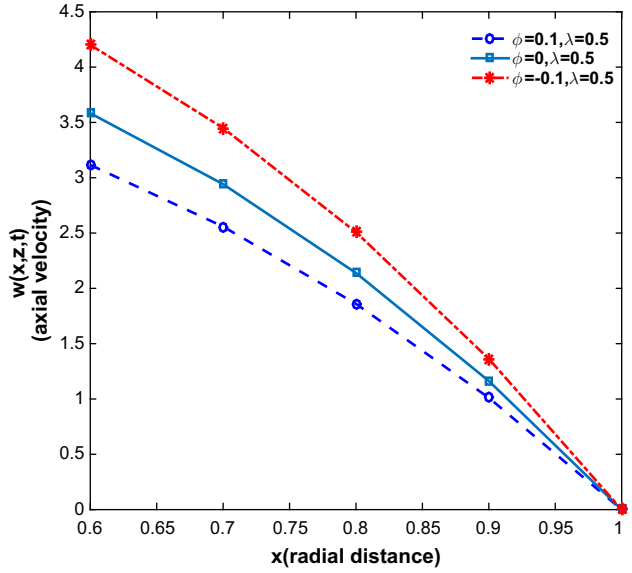


**Fig. 12** Axial velocity versus radial distances for $\phi = 0.1, 0, -0.1$ at $z = 28$, $\tau_y = 1.2$, $t = 0.45$, $K = 1.2$, $\lambda = 0.5$

near the boundary wall has also been expressed for changing λ-values. Owing to higher pressure gradient, required for blood to pass through constriction, the velocity for converging tapering is higher than for the cases of diverging and no-tapering. In addition, these graphs show that no-slip boundary condition is met for all three cases of converging, diverging and no-tapering. A distinct change in the magnitude of axial velocity has been observed corresponding to the changes in parametric value λ. The axial velocity decreases considerably for smaller values of λ.

In Figs. 14, 15, and 16, a comparison of axial velocity has been made against radial distance for Power law fluid, Newtonian fluid models with Thixotropic fluid model for the cases of converging, diverging, and no-tapering at the position $z = 28$ and time $t = 0.45$. It is noted that the magnitude of axial velocity for Power law fluid is smallest and magnitude of axial velocity for Newtonian fluid is almost coinciding with Thixotropic fluid for $\lambda = 0.1$. Observing the substantial increase in axial velocity for higher λ values and

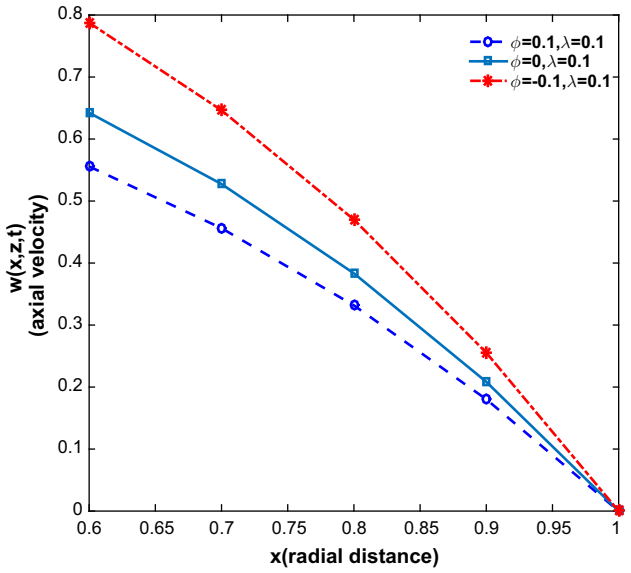


**Fig. 13** Axial velocity versus radial distances for $\phi = 0.1, 0, -0.1$ at $z = 28$, $\tau_y = 1.2$, $t = 0.45$, $K = 1.2$, $\lambda = 0.1$

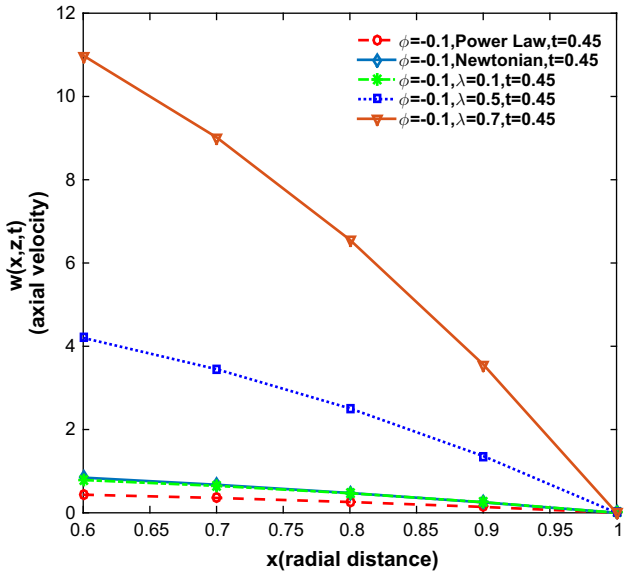


**Fig. 14** Axial velocity versus radial distances (near wall) for $\phi = -0.1$, $\lambda = 0.7, 0.5$, Power law model ($\lambda \to 0$) and Newtonian fluid ($\lambda \to 0$, $\mu = 0.035$, $n = 1$) at $z = 28$, $t = 0.45$, $\tau_y = 1.2$, $K = 1.2$

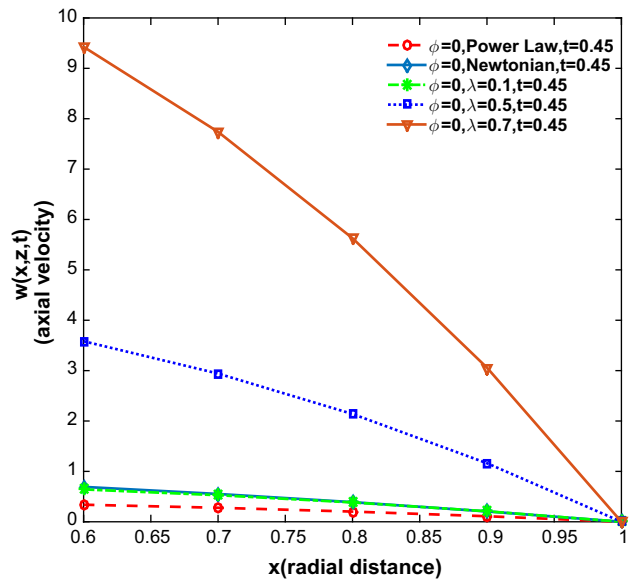


**Fig. 15** Axial velocity versus radial distances (near wall) for $\phi = 0$, $\lambda = 0.7, 0.5$, Power Law model ($\lambda \to 0$) and Newtonian fluid ($\lambda \to 0$, $\mu = 0.035$, $n = 1$) at z=28, t=0.45, $\tau_y = 1.2$, K=1.2

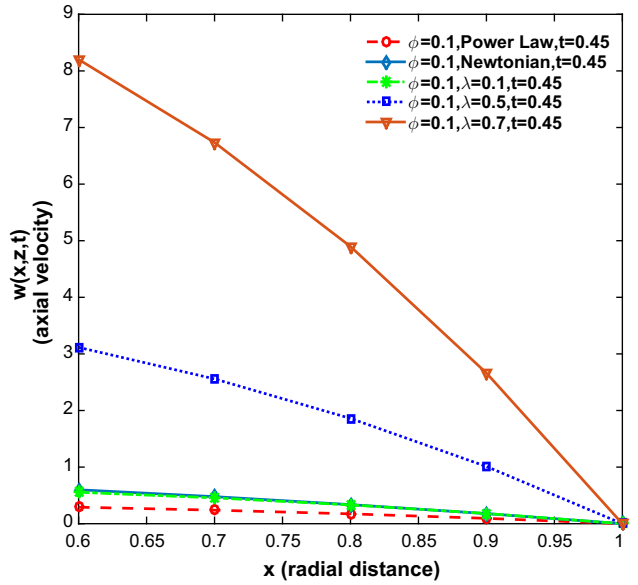


**Fig. 16** Axial velocity versus radial distances (near wall) for $\phi = 0.1$, $\lambda = 0.7, 0.5$, Power Law model ($\lambda \to 0$) and Newtonian fluid ($\lambda \to 0$, $\mu = 0.035$, $n = 1$) at $z = 28$, $t = 0.45$, $\tau_y = 1.2$, $K = 1.2$

the comparison with Herschel–Bulkley model study [46], it can be stated that our Thixotropic fluid model velocity can match experimental axial velocity for higher values of λ. In these images, the flatness of bottom curves corresponding to Newtonian, Power law and Thixotropic model for $\lambda = 0.1$ has been merely due to higher magnitude differences of axial velocity in comparison with magnitude of axial velocity for Thixotropic model for higher values of λ (= 0.5, 0.7).

Figures 17, 18 and 19 show the changes in flow resistance against time for converging tapering at a position of stenosis. The flow resistance increases sharply at earlier times, and then it begins to decrease slowly, approaching a certain magnitude after a while. The earlier rise in flow resistance can be associated with higher pressure gradient, required initially for fluid to propagate through compounding constriction and the later decline in flow resistance is contributed by lesser

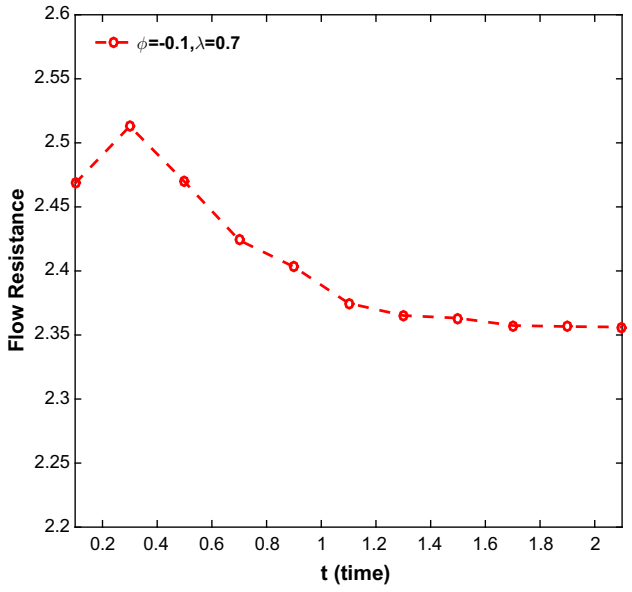


**Fig. 17** Flow resistance versus time for $\phi = -0.1$ at $z = 28$, $\tau_y = 1.2$, $K = 1.2$, $\lambda = 0.7$

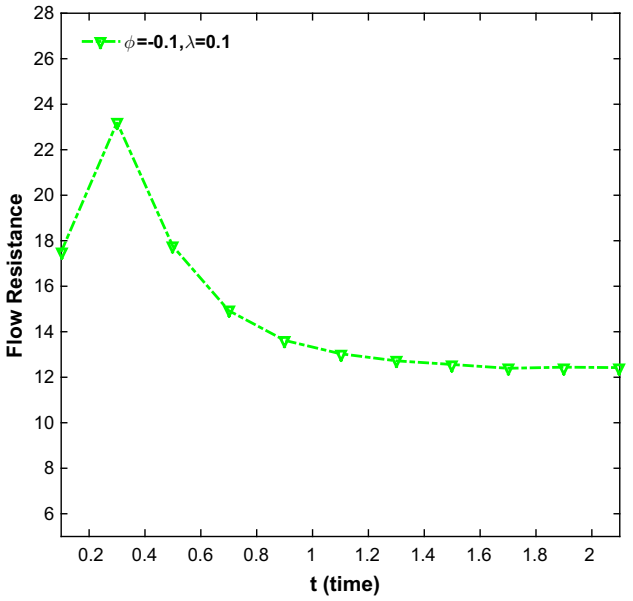


**Fig. 19** Flow resistance versus time for $\phi = -0.1$ at $z = 28$, $\tau_y = 1.2$, $K = 1.2$, $\lambda = 0.1$

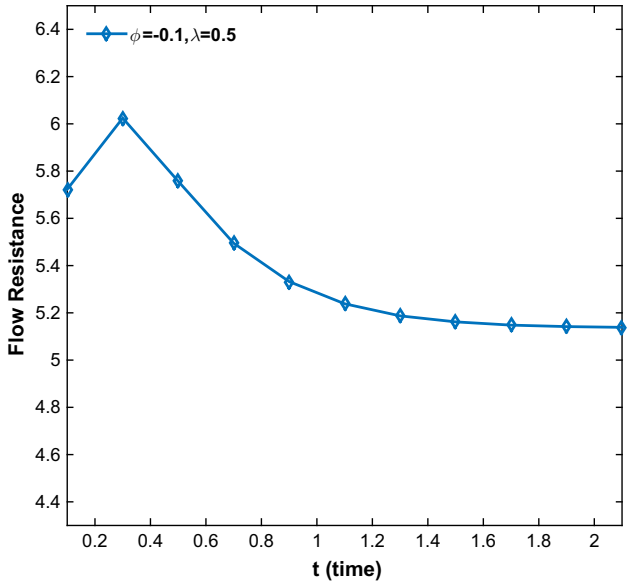


**Fig. 18** Flow resistance versus time for $\phi = -0.1$ at $z = 28$, $\tau_y = 1.2$, $K = 1.2$, $\lambda = 0.5$

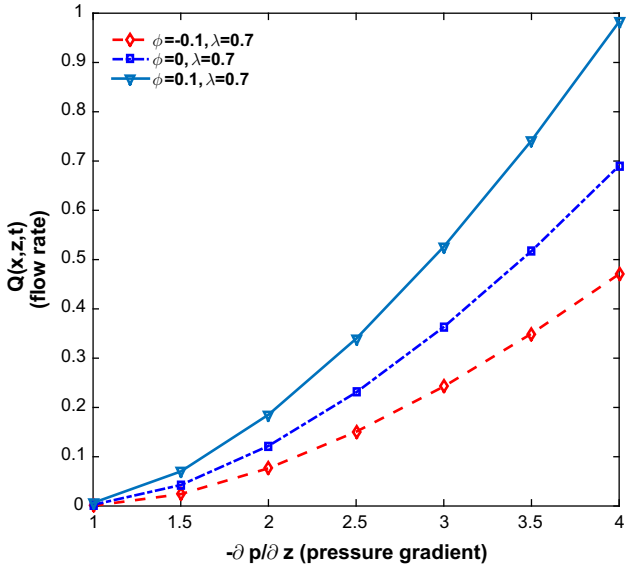


**Fig. 20** Flow rate versus pressure gradient for $\phi = -0.1, 0, 0.1$ at $z = 28$, $t = 0.45$, $\tau_y = 1.2$, $K = 1.2$, $\lambda = 0.7$

pressure gradient and slow movement of channel wall with increasing time. It is noted that the magnitude of resistance to flow increases for smaller values of λ and vice versa.

Figures 20, 21 and 22 illustrate the variation of flow rate corresponding to changes in pressure gradient for different values of λ . A slight nonlinear increase in flow rate with increase in pressure gradient has been observed. The highest flow rate curve for the case of diverging tapering is reflective of wider channel, giving way to substantial fluid to propagate, in comparison with the straight or narrowing channel (converging tapering) that hinders the flow. It is also noted that flow rate decreases considerably for small values of λ and increases for higher values of λ. This phenomenal finding also sits well with lesser flow resistance for bigger λ-values.

Figures 23, 24 and 25 reflect on effects of varying yield stress on axial velocity of fluid for corresponding changes in radial distance. These figures demonstrate the increase in magnitude of axial velocity with decrease in yield stress for

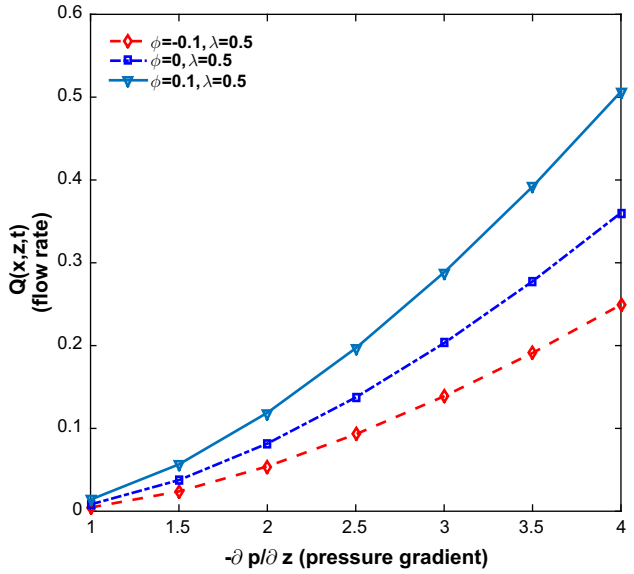


**Fig. 21** Flow rate versus pressure gradient for $\phi = -0.1, 0, 0.1$ at $z = 28, t = 0.45, \tau_y = 1.2, K = 1.2, \lambda = 0.5$

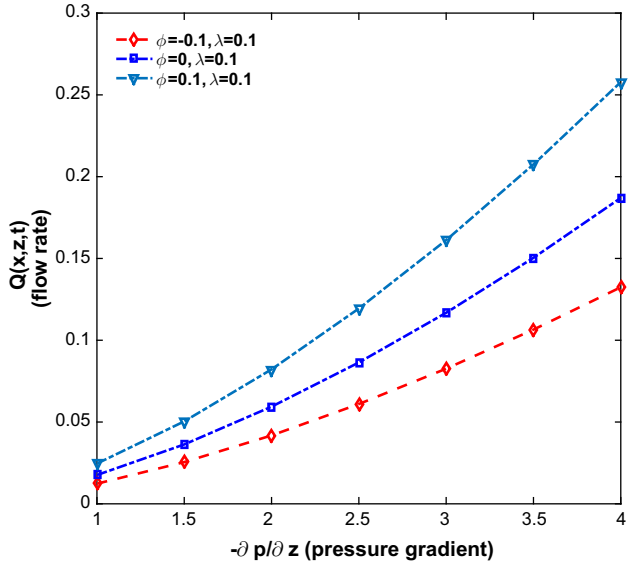


**Fig. 22** Flow rate versus pressure gradient for $\phi = -0.1, 0, 0.1$ at $z = 28, t = 0.45, \tau_y = 1.2, K = 1.2, \lambda = 0.1$

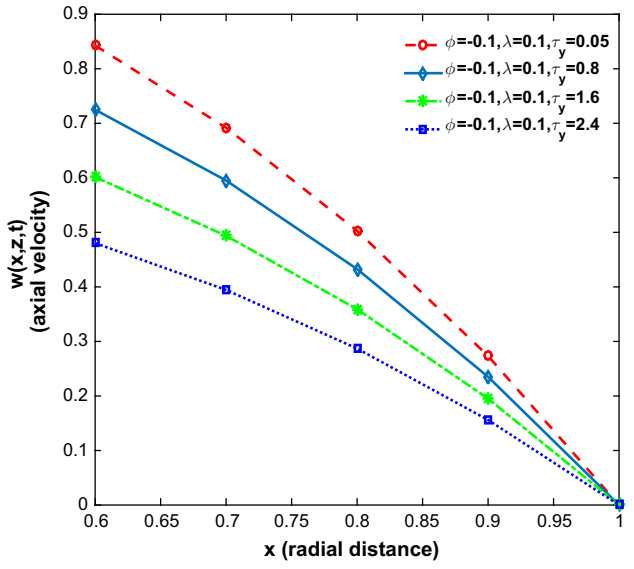


**Fig. 23** Axial velocity versus radial distances (near wall) for varying shear stress at $z = 28, t = 0.45, K = 1.2, \phi = -0.1, \lambda = 0.7$

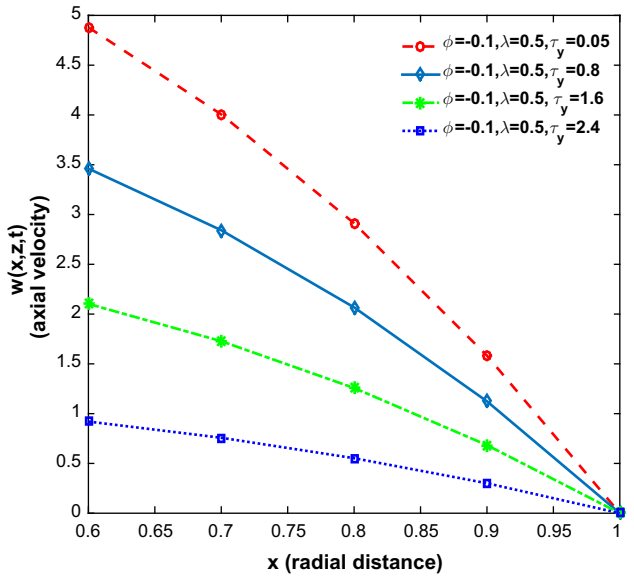


**Fig. 24** Axial velocity versus radial distances (near wall) for varying shear stress at $z = 28, t = 0.45, K = 1.2, \phi = -0.1, \lambda = 0.5$

the case of converging tapering. It is interesting to note that for small values of λ, the difference in magnitude of axial velocity at various radial distances for different values of yield stress is smaller as compared to magnitude of velocity for higher values of λ. This fact is manifested in the curves (for different yield stress values) being farther apart for the cases of $\lambda = 0.5, 0.7$ than for $\lambda = 0.1$. These images also show the verification of no-slip boundary condition for axial velocity.

## 7 Conclusions

The current analysis has been prepared to study the variation of dynamics of blood flow through a stenosed tapered artery due to a structural parameter λ of Thixotropic model. The inclusion of time parameter has allowed to analyse the model's suitability in a broader scheme. Following points of understanding have been observed through analytical and numerical computations in the simulated region $R_{\text{pc}} \leq x \leq R(z, t)$:

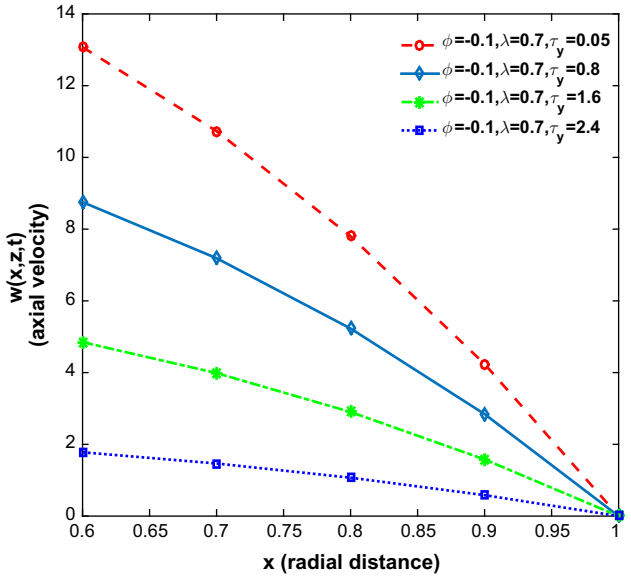


**Fig. 25** Axial velocity versus radial distances (near wall) for varying shear stress at $z = 28, t = 0.45, K = 1.2, \phi = -0.1, \lambda = 0.1$

1. The analytical expression of shear stress depends on time $t$, radial distance $x$ and numerically obtained values of pressure gradient. The shear stress at a stenosed position of artery continues to increase with respect to radial distance, reaching higher magnitude near the wall of vessel. However, an observation of data points of shear stress with respect to time demonstrates an increasing and decreasing pattern, hinting at oscillating variation of shear stress. The dependence of shear stress on model parameter $\lambda$ has also been studied to show that shear stress increases for increasing values of $\lambda$ in the range $0 < \lambda < 1$ and vice versa. An analysis of classification of shear stress on basis of diverging, converging and no-tapering artery shows that higher magnitude of shear stress is attained for converging tapering as compared to the other two cases.
2. An expression of axial velocity has been obtained by means of analytical computations. The observation of changes in axial velocity against radial distance, more specifically near the wall of vessel, was made. Due to constriction of channel, the axial velocity continues to decrease, approaching zero magnitude at the boundary wall of vessel. However, higher axial velocity for converging tapering as compared to other cases is explained by increased pressure gradient, required for flow propagation through narrow passage. A direct dependence of axial velocity on parameter $\lambda$ has been observed. The magnitude of velocity increases with increase in $\lambda$ and vice versa.
3. The approximation of velocity for Power law fluid model and Newtonian fluid model was obtained by considering $\lambda \to 0$ and $\lambda \to 0$ with $\mu = 0.035$, respectively, for converging, diverging and no-tapering of artery. Confirming the fact of declining magnitude of velocity for decreasing values of $\lambda$, the profile of axial velocity for Newtonian fluid was observed to be below the profiles for $\lambda = 0.7$ and $\lambda = 0.5$ and almost coinciding with the profile for $\lambda = 0.1$. Through graphical illustration, it is shown that, in comparison with Herschel–Bulkley fluid model, thixotropic fluid model can help to compare experimental conclusions with theoretical results by choosing right $\lambda$ value such that its influence on pressure gradient, velocity, shear stress and flow resistance can be studied to define better blood flow mechanism.
4. A comparison with axial velocity profiles in figure 3 [46] shows that our velocity profile for $0.1 \leq \lambda \leq 0.5$ (say) can be considered more closer to the experimental observations as compared to Herschel–Bulkley model.
5. For the case of converging tapering of artery, resistance to flow increases sharply at the face of stenosis and then decreases due to combination of lesser pressure gradient and slower movement of vessel wall with time. Also resistance to flow decreases for increasing values of $\lambda$ and vice versa.
6. The existence of a direct relation between pressure gradient and flow rate has been verified in accordance with available results [46,49]. For the case of fixed yield stress, unlike the case of flow resistance, the flow rate is directly affected by parameter $\lambda$ that is it decreases for decreasing values of $\lambda$ and vice versa.
7. The study of effects of rising yield stress confirms the decreased magnitude of axial velocity for converging tapering. The effects of parameter $\lambda$ on these graphs are more evident because of higher magnitude of velocity in the range $0.5 \leq \lambda < 1$.

**Acknowledgements** The author thanks Dr. Howard Stone from Department of Mechanical and Aerospace Engineering, Princeton University for his insightful discussion on topic and Princeton University for providing a wonderful working atmosphere for completion of this project.

## References

1. Young, D.F.: Effect of a time dependent stenosis of flow through a tube. J. Eng. Ind. **90**, 248–254 (1968)
2. Young, D.F.: Fluid mechanics of arterial stenoses. J. Biomech. Eng. **101**(3), 157–175 (1979)
3. Young, D.F.; Tsai, F.Y.: Flow characteristics in models of arterial stenoses: I. Steady flow. J. Biomech. **6**(4), 395–410 (1973)
4. Shahed, M-El: Pulsatile flow of blood through a stenosed porous medium under periodic body acceleration. Appl. Math. Comput. **138**(2–3), 479–488 (2003)
5. Elshehawey, E.F.; Elbarbary, E.M.; Affifi, N.A.S.; Shahed, M-El: Pulsatile flow of blood through a porous medium under periodic body acceleration. Int. J. Theor. Phys. **39**(1), 183–188 (2000)

6. Sharma, M.K.; Bansal, K.; Bansal, S.: Pulsatile unsteady flow of blood through porous medium in a stenotic artery under the influence of transverse magnetic field. Korea Aust. Rheol. J. **24**(3), 181–189 (2012)
7. Tu, C.; Deville, M.; Dheur, L.; Vandershuren, L.: Finite element simulation of pulsatile flow through arterial stenosis. J. Biomech. **25**, 1141–1152 (1992)
8. Nerem, R.E.: Vascular fluid mechanics, the arterial wall and arteriosclerosis. J. Biomech. Eng. Trans. ASME **114**, 274–282 (1992)
9. Cavalcanti, S.: Hemodynamics of an artery with mild stenosis. J. Biomech. **28**, 387–399 (1995)
10. Siouffi, M.; Deplano, V.; Pelissra, R.: Experimental analysis of unsteady flows through a stenosis. J. Biomech. **31**, 11–19 (1997)
11. Zendehboodi, G.R.; Moayeri, M.S.: Comparison of physiological and simple pulsatile flows through stenosed arteries. J. Biomech. **32**, 959–965 (1999)
12. Chakravarty, S.; Mandal, P.K.: Two-dimensional blood flow through tapered arteries under stenotic conditions Int. J. Nonlinear Mech. **35**, 779–793 (2000)
13. Long, Q.; Ku, X.Y.; Ramnarine, K.V.; Hoskins, P.: Numerical investigation of physiologically realistic pulsatile flow through arterial stenosis. J. Biomech. **34**, 1229–1242 (2001)
14. Smith, F.T.: The separation flow through a severely constricted symmetric tube. J. Fluid Mech. **90**, 725–754 (1979)
15. Deshpande, M.D.; Giddens, P.D.; Mabon, F.R.: Steady laminar flow through modelled vascular stenoses. J. Biomech. **9**, 165–174 (1976)
16. Mandal, P.K.; Chakravarty, S.; Mandal, A.; Amin, N.: Effect of body acceleration on unsteady pulsatile flow of non-Newtonian fluid through a stenosed artery. Appl. Math. Comput. **189**(1), 766–779 (2007)
17. Mansour, R.B.; Badr, H.; Shaik, A.Q.; Maalej, N.: Modeling of pulsatile blood flow in an axisymmetric tube with a moving indentation. Arab. J. Sci. Eng. **33**(1), 5 (2008)
18. Das, K.: A mathematical model on the consistency coefficient of the Herschel–Bulkley flow of blood through narrow vessel arab. J. Sci. Eng. **36**, 405 (2011). https://doi.org/10.1007/s13369-011-0040-1
19. Ponalagusamy, P.: Mathematical analysis on effect of non-Newtonian behavior of blood on optimal geometry of microvascular bifurcation system. J. Frankl. Inst. **349**(9), 2861–2874 (2012)
20. Ponalagusamy, P.: Pulsatile flow of Herschel–Bulkley fluid in tapered blood vessels. In: Proceedings of the International Conference Science Computing, and World Congress in Computer Science, Computer Engineering and Applied Computing, pp 67–73 (2013)
21. Liepsch, D.; Moravec, S.T.: Pulsatile flow of non-Newtonian fluid in distensible models of human arteries. Biorheology **21**, 571–586 (1984)
22. Chakravarty, S.: Effects of stenosis on the flow behaviour of blood in an artery Int. J. Eng. Sci. **25**, 1003–1016 (1987)
23. Nakamura, M.; Swada, T.: Numerical study on the flow of a non-Newtonian fluid through an axisymmetric stenosis. J. Biomech. Eng. Trans. ASME **110**, 137–143 (1988)
24. Nakamura, M.; Swada, T.: Numerical study on the unsteady flow of non-Newtonian fluid. J. Biomech. Eng. Trans. ASME **112**, 100–103 (1990)
25. Pak, B.; Young, Y.I.; Choi, S.U.S.: Separation and re-attachment of non-Newtonian fluid flows in a sudden expansion pipe. J. Non-Newton. Fluid Mech. **37**, 175–199 (1990)
26. Misra, J.C.; Patra, M.K.; Misra, S.C.: A non-Newtonian fluid model for blood flow through arteries under stenotic conditions. J. Biomech. **26**, 1129–1141 (1993)
27. Tu, C.; Deville, M.: Pulsatile flow of non-Newtonian fluid through arterial stenosis. J. Biomech. **29**, 899–908 (1996)
28. Das, B.; Johnson, P.C.; Popel, A.S.: Effect of non axisymmetric hematocrit distribution on non-Newtonian blood flow in small tubes. Biorheology **35**, 69–87 (1998)
29. Bureau, M.; Healy, J.C.; Bourgoin, D.; Joly, M.: Etude rheologique en regime transitoire de quelques echantillons de sangs humains artificiellement modifies. Rheol. Acta **18**, 756–768 (1979)
30. Bureau, M.; Healy, J.C.; Bourgoin, D.; Joly, M.: Rheological hysteresis of blood at low shear rate. Biorheology **17**, 191–203 (1980)
31. Dintenfass, L.: Thixotropy of blood and proneness to thrombus formation. Circ. Res. **11**, 233–239 (1962)
32. Cokelet, G.R.; Merrill, E.W.; Gilliland, E.R.; Shin, H.; Britten, A.; Wells, E.R.: The rheology of human blood measurement near and at zero shear rate. Trans. Soc. Rheol. **7**, 303–317 (1963)
33. Chien, S.; Usami, S.; Taylor, H.M.; Lundberg, J.L.; Gregerse, M.I.: Effects of hematocrit and plasma proteins on human blood rheology at low shear rates. J. Appl. Physiol. **21**, 81–87 (1966)
34. Merrill, E.W.; Benis, A.M.; Gillian, E.R.; Sherwood, T.K.; Salzman, E.W.: Pressure-flow relations of human blood in hollow fibers at low rates. J. Appl. Physiol. **20**, 954–967 (1965)
35. Merrill, E.W.; Pelletier, G.A.: Viscosity of human blood: transition from Newtonian to non-Newtonian. J. Appl. Physiol. **23**, 178–182 (1967)
36. Merrill, E.W.: Rheology of blood. Physiol. Rev. **49**, 863–888 (1969)
37. Thurston, G.B.: Elastic effects in pulsatile blood-flow. Microvasc. Res. **9**, 145–157 (1975)
38. Thurston, G.B.: Effects of frequency of oscillatory flow on impedance of rigid, blood-filled tubes. Biorheology **13**, 191–199 (1976)
39. Owens, R.G.: A new micro structure-based constitutive model for human blood. J. Non Newton. Fluid Mech. **140**, 57–70 (2006)
40. Fang, J.N.; Owens, R.G.: Numerical simulations of pulsatile blood flow using a new constitutive model. Biorheology **43**, 637–660 (2006)
41. Moyers-Gonzalez, M.; Owens, R.G.; Fang, J.N.: A non-homogeneous constitutive model for human blood. Part 1. Model derivation and steady flow. J. Fluid Mech. **617**, 327–354 (2008a)
42. Anand, M.J.; Rajagopal, K.: A shear-thinning viscoelastic fluid model for describing the flow of blood Int. J. Cardiovasc. Med. Sci. **4**, 59–68 (2004)
43. Anand, M.J.; Kwack, J.; Masood, A.: A new generalized Oldroyd-B model for blood flow in complex geometries Int. J. Eng. Sci. **72**, 78–88 (2013)
44. Pincombe, B.; Mazumdar, J.; Hamilton-Craig, I.: Effects of multiple stenoses and post-stenotic dilatation on non-Newtonian blood flow in small arteries. Med. Biol. Eng. Comput. **37**(5), 595–599 (1999)
45. Scott Blair, G.W.; Spanner, D.C.: An Introduction to Biorheology. Elsevier Scientific Publishing, Amsterdam (1974)
46. Priyadharshini, S.; Ponalagusamy, R.: Biorheological model on flow of Herschel–Bulkley fluid through a tapered arterial stenosis with dilatation. Appl. Bionic Biomech. (2015). https://doi.org/10.1155/406195
47. Whitemore, R.L.: Rheology of Circulation. Pergamon Press, Oxford (1968)
48. Manton, M.J.: Low Reynolds number flow in slowly varying axisymmetric tubes. J. Fluid Mech. **49**, 451–459 (1971)
49. Mandal, P.K.: An unsteady analysis of non-Newtonian blood flow through tapered arteries with a stenosis Int. J. Non Linear Mech. **40**(1), 151–164 (2005)
50. Mujumdar, A.; Anthony, N.B.; Metzner, A.B.: Transient phenomena in thixotropic systems. J. Non Newton. Fluid Mech. **102**, 157–178 (2002)
51. Dullaert, K.; Mewis, J.: A structural kinetics model for thixotropy. J. Non Newton. Fluid Mech. **139**, 21–30 (2006)
52. Mewis, J.; Wagner, N.J.: Colloidal Suspension Rheology. Cambridge University, Cambridge (2012)

53. Apostolidis, A.J.; Anthony, N.B.: Modelling of the blood rheology in steady-state shear flows. J. Rheol. **58**, 607–633 (2014)
54. Mewis, J.: Thixotropy: a general review. J. Non Newton. Fluid Mech. **6**, 1–20 (1979)
55. Bird, R.B.; Armstrong, R.C.; Hassager, O.: Dynamics of Polymeric Liquids 1 Fluid Mech. Wiley, New York (1977)
56. Apostolidis, A.J.; Armstrong, M.J.; Anthony, N.B.: Modelling of human blood rheology in transient shear flows. J. Rheol. **59**, 275–298 (2015)